16th World Congress in Computational Mechanics (WCCM)
21-26 July 2024, Vancouver, Canada
A. Korobenko, M. Laforest, S. Prudhomme, R. Vaziri (Eds)

NUMERICAL INVESTIGATION ON FLUID-FLEXIBLE-STRUCTURE INTERACTION BASED ON SPH METHOD

T. BAO[1], J. HU[2], C. HUANG[3], Y. YU[4] AND A. SHAKIBAEINIA[5]

[1] Beijing Institute of Technology, Beijing, China, 100081, baotingting@bit.edu.cn

[2] Beijing Institute of Technology, Beijing, China, 100081, hujun@bit.edu.cn

[3] North China University of Technology, Beijing, China, 100144, huangcancan@163.com

[4] Beijing Institute of Technology, Beijing, China, 100081, yuyong@bit.edu.cn

[5] Polytechnique Montreal, QC, Canada, H3T 1J4, ahmad.shakibaeinia@polymtl.ca

Key words: Smoothed particle hydrodynamics (SPH), Fluid-flexible-structure interaction (FFSI), Single-layer boundary, Shell model

Abstract. The fluid-flexible-structure interaction (FFSI) is characterized by the large deformation, the thin structure, and the complex of the flow field. Accurately simulating FFSI poses three challenges, which are the reproduction of thin structure, the capture of moving interface, and the numerical stability of multi-physics field coupling, respectively. In this study, the FFSI is simulated by the smoothed particle hydrodynamics (SPH) because of its natural advantage in dealing with the moving interface. The shell model with single-layer particles[1] is introduced into SPH to simulate the thin flexible structure. The truncation error caused by the single-layer boundary is modified by the normal flux approach[2]. κ-ε turbulence model is introduced into SPH to enhance the numerical stability and capture complex flow details. In addition, other techniques or models that ensure the efficiency and stability of the calculation are used in this study, including PST (particle shifting technique), δ-SPH method, and GPU (graphics processing unit). The flows around the single filament are simulated to verify the accuracy and stability of the current FFSI algorithm based on the SPH method.

1 INTRODUCTION

Fluid-flexible-structure interaction (FFSI) is widespread in nature and engineering practice, such as the flapping of flags in the wind, the swaying of the aquatic plants with the current, the vibration of high-voltage transmission lines in the wind, the heart valve response in blood flow, the oscillation of underwater cables induced by tides, and so on. FFSI is one particular form of fluid-structure interaction (FSI), which refers to the mutual coupling between moving fluid and thin flexible structure. In FFSI, the force of the fluid is exerted on the thin flexible structure to cause it to deform, and the deformed flexible structure affects the fluid boundary and thus changes the flow field. One of the main features that distinguishes FFSI from FSI is that the thin flexible structure has small bending stiffness and is prone to large deformation when interacting with the fluid, making the FFSI problem nonlinear and the coupling strong [3].

In recent years, the rapid development of computer technology has greatly aided the research of FFSI problems through computational simulation methods. Among them, the smoothed particle hydrodynamics (SPH) is a very suitable method for simulating FFSI because of its meshless advantage in capturing the moving interface and large deformation within a unified framework [4]. A large number of studies have focused on the SPH-FEM coupling application [5–8], that is, using the SPH method to solve the fluid dynamics and the FEM method to solve the structural dynamics. However, the SPH-FEM coupling method is limited due to the extremely high computational cost in the contact searching process used to recognize the contact interface between fluid and structure [5]. In addition, once the structure undergoes large deformation, it needs to be re-meshed, which will increase the algorithm complexity and the computational cost. The works of a unified SPH framework can be found in the simulation of FSI problems [9–14], where the structure is treated as a thick beam model. As mentioned before, the main feature of FFSI problems is the thin flexible structure, which will undergo large deformation due to the hydrodynamic force acting on it. There is a significant knowledge gap in solving FFSI problems using the purely and fully SPH method within a unified framework, in which the structure is considered as the SPH thin shell model. As for the SPH method simulating the thin structure, Wu et al. [1] made great improvements to the shell model with the reduced-dimensional SPH method while Li et al. [2] proposed a model to calculate the information of fluid particles near the single-layer particle wall boundary. Inspired by the above works, this study combines methods of the shell structural model and the single-layer effect in fluid to apply the proposed pure SPH algorithm in FFSI simulations.

The paper is structured as follows: Section 2 presents the numerical methods, with a focus on SPH discretization, fluid dynamics, and shell structural dynamics. Section 3 is dedicated to presenting some simulation results of the filament. Finally, Section 4 offers the conclusions of the study.

2 METHODOLOGIES

2.1 SPH method

In the general SPH discretization, the field function $f(\boldsymbol{x_a})$ and its gradient $\nabla f(\boldsymbol{x}_a)$ of particle a located at the spatial coordinate $\boldsymbol{x_a}$ can be approximated by kernel function W and its gradient ∇W [15,16].

$$f(\boldsymbol{x_a}) = \sum_b f(\boldsymbol{x_b}) W_{ab} V_b \tag{1}$$

$$\nabla f(\boldsymbol{x_a}) = \sum_b f(\boldsymbol{x_b}) \nabla_a W_{ab} V_b \tag{2}$$

where a and b indicate a pair of interacting particles; $\boldsymbol{x}_b$ is the spatial coordinates of the neighboring particle b; V_b is the volume of particle b, $V_b = m_b/\rho_b$; m_b and ρ_b are the mass and density of particle b, respectively; W_{ab} is the smooth kernel function (also called kernel function); $\nabla_a W_{ab}$ is the gradient of the kernel function. In this study, the Gaussian kernel function is adopted in the fluid solver,

$$W = \alpha_d \begin{cases} e^{-R^2}, & 0 \le R < 3 \\ 0, & R \ge 3 \end{cases} \tag{3}$$

where R is the dimensionless distance between adjacent particles, $R=|\boldsymbol{r}_a- \boldsymbol{r}_b|/h$, and h is the smooth length. In the two-dimensional plane, the coefficient α_d is $1/(\pi h^2)$. The Gaussian kernel function has a large support domain, which can ensure that there are enough adjacent particles to participate in the calculation and effectively improve the calculation accuracy [17].

The Wenland C2 kernel function is used in the flexible structure solver,

$$W = \alpha_d \begin{cases} (1+2R)(1-R/2)^4, 0 \le R < 2 \\ 0, \quad R \ge 2 \end{cases} \tag{4}$$

where the coefficient α_d =3/(4h) in this study for two-dimensional structure.

2.2 The modification of the single-layer boundary

In this study, to simulate the SPH shell model, the structure is modeled by single-layer particles. The structure is also the boundary of the fluid, which means the positions where structural particles are located also belong to the positions of boundary particles in the fluid. The single-layer shell structure means the single-layer boundary, whose challenge is the truncation of the support domain of fluid particles near the boundary. In this study, we utilize the normal flux approach, as proposed by Li et al. [2], which considers a modification of kernel function for fluid particles near the boundary. The integral approximation of the spatial derivative $\nabla f(\boldsymbol{x})$ can be modified as follows:

$$\nabla f(\boldsymbol{x}_a) = \sum_m [f(\boldsymbol{x}_m) - f(\boldsymbol{x}_a)]\, W(\boldsymbol{x}_a - \boldsymbol{x}_m, h) \cdot n_m S_m + \sum_b [f(\boldsymbol{x}_b) - f(\boldsymbol{x}_a)]\, \nabla_a W(\boldsymbol{x}_a - \boldsymbol{x}_b, h) V_b \tag{5}$$

where m represents the single-layer boundary particle within the support domain of fluid particle a; b represents the fluid particle within the support domain of fluid particle a; $\boldsymbol{n}_m$ is the normal vector of the single-layer boundary particle m. S_m is the area of particle m. In two-dimensional space, here S_m is equal to particle spacing Δ.

2.3 Fluid solver

The governing equations of fluid dynamics including the turbulence model can be expressed as follows:

$$\frac{D\rho}{Dt} = -\rho \frac{\partial u_i}{\partial x_i} \tag{6}$$

$$\rho \frac{Du_i}{Dt} = -\frac{\partial p}{\partial x_i} + \frac{\partial}{\partial x_j}\left(\mu \frac{\partial u_i}{\partial x_j} - \rho \overline{u_i' u_j'}\right) + \boldsymbol{f}^{ext} \tag{7}$$

where i, j are the indexes representing different directions; t is the time; D/Dt indicates the global derivative; ρ is the density; u_i, u_j are the time-averaged value of the velocity components; p is the time-averaged pressure; μ is the dynamic viscosity of fluid; $-\rho\overline{u_i' u_j'}$ is the Reynolds stress; $\boldsymbol{f}^{ext}$ is the external force, including gravity and resistance, $\boldsymbol{f}^{ext} = \rho\boldsymbol{g} - \beta\boldsymbol{u}$ in this study where $\boldsymbol{g}$ is gravity and $\boldsymbol{u}$ is the velocity of fluid. Herein, β is the coefficient of the resistance, calculated as $\beta\boldsymbol{u}_0 = \rho_0\boldsymbol{g}$ [18], where $\boldsymbol{u}_0$ is the inlet velocity.

When solving the pressure p in Eq. (7), a weakly compressible state equation is used,

$$p = B\left[\left(\frac{\rho}{\rho_0}\right)^{\gamma} - 1\right] \tag{8}$$

where coefficient $B = \rho_0 c^2 / \gamma$, $\gamma = 7.0$; ρ_0 is the initial or reference density; c is the artificial sound speed that ensures calculation efficiency and stability. To ensure the weakly compressible conditions, it is necessary to limit the inflow Mach number *Ma* (that is, the ratio of the inflow velocity to the artificial sound speed) to not be greater than 0.1. Generally in the SPH calculation, the sound speed c is set as $c \geq 10\max(u_{\max}, \sqrt{p_{\max}/\rho_0})$ [19,20], where $u_{\max}$ and $p_{\max}$ are the estimated maximum fluid velocity and pressure, respectively.

The Reynolds stress in Eq. (7) is calculated as follows:

$$-\rho\overline{u_i' u_j'} = (\tau_{i,j})_t = -p_t\delta_{i,j} + \mu_t\left(\frac{\partial u_i}{\partial x_j} + \frac{\partial u_j}{\partial x_i}\right) - \frac{2}{3}\mu_t\delta_{i,j}divu \tag{9}$$

where p_t is the pressure caused by the fluctuation, $p_t = \frac{2}{3}\frac{\rho_0}{\gamma}\left[\left(\frac{\rho}{\rho_0}\right)^{\gamma} - 1\right]k$; μ_t is the turbulent viscosity coefficient shown as follows:

$$\mu_t = c_\mu \rho k^2/\varepsilon \tag{10}$$

where k is the turbulent kinetic energy; ε is the dissipation rate. The equations about turbulent kinetic energy k and dissipation rate ε are calculated by[21]

$$\rho\frac{Dk}{Dt} = \frac{\partial}{\partial x_j}\left[\left(\mu + \frac{\mu_t}{\sigma_k}\right)\frac{\partial k}{\partial x_j}\right] + \mu_t\frac{\partial u_i}{\partial x_j}\left(\frac{\partial u_i}{\partial x_j} + \frac{\partial u_j}{\partial x_i}\right) - \rho\varepsilon \tag{11}$$

$$\rho\frac{D\varepsilon}{Dt} = \frac{\partial}{\partial x_j}\left[\left(\mu + \frac{\mu_t}{\sigma_\varepsilon}\right)\frac{\partial \varepsilon}{\partial x_j}\right] + \frac{c_1\varepsilon}{k}\mu_t\frac{\partial u_i}{\partial x_j}\left(\frac{\partial u_i}{\partial x_j} + \frac{\partial u_j}{\partial x_i}\right) - c_2\rho\frac{\varepsilon^2}{k} \tag{12}$$

The coefficients in the Eqs. (9), (10), (11) and (12) are $c_\mu = 0.09$, $c_1 = 1.44$, $c_2 = 1.92$, $\sigma_k = 1.0$, and $\sigma_\varepsilon = 1.3$.

The governing equations (6), (7), (11), and (12) are discretized by the SPH method, as shown in Eqs. (1) and (2). In addition, for fluid particles near the single-layer boundary, the modified format considering the effect of single-layer is added according to Eq (5).

Please note that in this algorithm, some techniques or models that ensure the efficiency and stability of the calculation are used. To suppress the oscillation of the density and pressure, the δ-SPH model [22] is introduced in the continuity discretization equation. To avoid the particle aggregation and cavitation phenomena, the particle shifting technique (PST) is introduced to enhance the calculation stability of the particle method in the Lagrangian space [23].

2.4 Flexible-structure solver

In this study, the SPH shell model with a single layer is adopted to construct the thin structure, ensuring accurate modeling of the thin structure while minimizing the computational cost.

According to the Uflyand-Mindlin theory, the shell structure behavior can be represented by using one layer of particles at the mid-surface of the shell. In the SPH shell model, there are

such coordinates: global coordinate $\boldsymbol{X}=(X,Y,Z)$, initial local coordinate $\boldsymbol{x}^0=(x^0,y^0,z^0)$, and current local coordinate $\boldsymbol{x}=(x,y,z)$. Each SPH particle possesses five degrees of freedom: three translations $\boldsymbol{q}=\{q_1,q_2,q_3\}^T$ and two rotations $\boldsymbol{\theta}=\{\theta,\varphi\}^T$, expressed in the initial configuration tangent to the initial shell mid-surface. The pseudo-normal vector is presented in initial coordinates $\boldsymbol{n}=\{n_1,n_2,n_3\}^T$.

The plate is assumed to have a uniform thickness *d*. The position vector $\boldsymbol{r}$ of any material point located at a distance z^0 from the mid-surface can be expressed as

$$\boldsymbol{r}(x^0,y^0,z^0,t)=\boldsymbol{r_m}(x^0,y^0,t)+z^0\boldsymbol{n}(x^0,y^0,t),\quad z^0\in[-d/2,d/2] \tag{13}$$

where $\boldsymbol{r_m}$ is the position vector of the particle located on the mid-surface. In the following text, the subscript $(\bullet)_m$ represents the parameter on the mid-surface of the shell.

The displacement vector expressed in the initial local coordinate can be expressed as follows:

$$\boldsymbol{q}(x^0,y^0,z^0,t)=\boldsymbol{q_m}(x^0,y^0,t)+z^0\boldsymbol{\Delta n}(x^0,y^0,t) \tag{14}$$

The deformation gradient tensor **F** is defined by

$$\mathbf{F}=\nabla^0\boldsymbol{r}=\{\boldsymbol{a_1}^T,\boldsymbol{a_2}^T,\boldsymbol{a_3}^T\} \tag{15}$$

where,

$$\begin{aligned}\boldsymbol{a_1}&=\boldsymbol{r}_{m,x^0}+\zeta\boldsymbol{n}_{x^0}\\ \boldsymbol{a_2}&=\boldsymbol{r}_{m,y^0}+\zeta\boldsymbol{n}_{y^0}\\ \boldsymbol{a_3}&=\boldsymbol{n}\end{aligned} \tag{16}$$

Therefore, the deformation gradient tensor can be split into two parts.

$$\mathbf{F}=\mathbf{F}_m+z^0\mathbf{F}_n \tag{17}$$

where $\mathbf{F}_m=\left(\boldsymbol{r}_{m,x^0}{}^T,\boldsymbol{r}_{m,y^0}{}^T,\boldsymbol{n}^T\right)$ and $\mathbf{F}_n=\left(\boldsymbol{n}_{x^0}{}^T,\boldsymbol{n}_{y^0}{}^T,0\right)$.

In the shell model, Green-Lagrange strain tensor **E** can be described by the deformation gradient tensor **F** :

$$\mathbf{E}=\mathbf{0.5}(\mathbf{F^TF}-\mathbf{I}) \tag{18}$$

Euler-Almansi strain tensor can be written as follows:

$$\boldsymbol{\varepsilon}_{\mathbf{alm}}=\mathbf{F^{-T}EF^{-1}}=\mathbf{0.5}(\mathbf{I}-\mathbf{F^{-T}F^{-1}}) \tag{19}$$

The constitutive relation is established via the Euler-Almansi strain and Caushy stress $\boldsymbol{\sigma}$ in the local coordinate of the current configuration:

$$\boldsymbol{\sigma}=K\mathbf{tr}(\boldsymbol{\varepsilon})\mathbf{I}+2G\left(\boldsymbol{\varepsilon}-\frac{1}{3}\mathrm{tr}(\boldsymbol{\varepsilon})\mathbf{I}\right)=\lambda\mathrm{tr}(\boldsymbol{\varepsilon})\mathbf{I}+2\mu\boldsymbol{\varepsilon} \tag{20}$$

where the shear modulus $G=\dfrac{E}{2(1+\nu)}$; the bulk modulus $K=\dfrac{E}{3(1-2\nu)}$; *E* denotes the Young's modulus and ν denotes the Poisson ratio; λ and μ are Lamè constants, $\lambda=K-2\mu/3$, $\mu=G$.

The second-order Piola-Kirchhoff stress tensor **S** is expressed in the current local coordinate as follows:

$$\mathbf{S} = J\mathbf{F}^{-1}\mathbf{Q}^{0}\mathbf{Q}^{\mathrm{T}}\boldsymbol{\sigma}\mathbf{Q}(\mathbf{Q}^{0})^{\mathrm{T}}\mathbf{F}^{-\mathrm{T}} \tag{21}$$

where $J = \det(\mathbf{F}_m)$ is the Jacobian determinant, $\mathbf{Q}^0$ and $\mathbf{Q}$ are orthogonal transformation matrices in the initial local coordinate and current local coordinate, respectively.

The first-order Piola-Kirchhoff stress tensor **P** can be expressed as

$$\mathbf{P} = \mathbf{Q}(\mathbf{Q}^{0})^{\mathrm{T}}\mathbf{F}\mathbf{S} \tag{22}$$

Based on the three-point Gaussian quadrature rule, the Piola-Kirchhoff stress tensor obtained by the above formula is summed to obtain the generalized stress tensor **N** and the generalized moment tensor **M** in the initial local coordinate as follows:

$$\mathbf{N} = \int_{-d/2}^{d/2} \mathbf{P}(z^0)dz^0 = \frac{d}{2}\int_{-1}^{1} \mathbf{P}(\frac{d}{2}z^0)dz^0 = \frac{d}{2}\sum_{k=1}^{3} \mathbf{P}(\frac{d}{2}z_k^0)\alpha_k \tag{23}$$

$$\mathbf{M} = \int_{-d/2}^{d/2} z^0\mathbf{P}(z^0)dz^0 = \frac{d}{2}\int_{-1}^{1} \frac{d}{2}z^0\mathbf{P}(\frac{d}{2}z^0)dz^0 = \frac{d}{2}\sum_{k=1}^{3} \frac{d}{2}z_k^0\mathbf{P}(\frac{d}{2}z_k^0)\alpha_k \tag{24}$$

In this study, the Gaussian sampling point positions are selected as z_k^0 = (0, 0.7746, -0.7746), which are located on the mid-surface and its two sides, respectively. The integration weights corresponding to the sampling points are α_k = (0.8889, 0.5556, -0.5556).

The mass conservation equation of the shell model is

$$\rho = J_m^{-1}\rho^0 \tag{25}$$

where $J_m^{-1} = \det(\mathbf{F}_m)$, ρ^0 and ρ are the structure densities at the initial and current time respectively.

The dynamic equations described in TL-SPH can be written as

$$d\rho^0\ddot{\boldsymbol{q}}_{\boldsymbol{m}} = \nabla\cdot(\mathbf{N}^{\mathbf{T}}) + \boldsymbol{F}^{\boldsymbol{ext}} \tag{26}$$

$$\frac{d^3}{12}\rho^0\ddot{\boldsymbol{n}} = \nabla\cdot(\mathbf{M}^{T}) + \mathbf{T} \tag{27}$$

$\boldsymbol{F}^{ext}$ is the external force acting on the shell structure, including gravity $\boldsymbol{g}$ and the interaction force of fluid-flexible structure $\boldsymbol{f}^{interac}$. The fluid-flexible-structure interaction force $\boldsymbol{f}^{interac}$ represents the external force exerted by the fluid on the flexible structure.

$$\boldsymbol{f}^{interac} = d\rho^0\left(\left(\frac{Du_i}{Dt}\right)_{fluid} - \boldsymbol{f}_{fluid}^{ext}/\rho_{fluid}\right) \tag{28}$$

The discretization format of the dynamic equations can be written as

$$\ddot{\boldsymbol{q}}_{m,a} = \sum_b (\mathbf{N_a} + \mathbf{N}_b)\cdot\frac{\nabla_a^0 W_{ab}V_b}{d\rho_a^0} + \frac{\boldsymbol{F}_a{}^{ext}}{d\rho_a^0} \tag{29}$$

$$\ddot{\boldsymbol{n}}_a = \sum_b (\mathbf{M}_a + \mathbf{M}_b) \cdot \frac{12\nabla_a^0 W_{ab} V_b}{d^3 \rho_a^0} + \frac{12\mathbf{T}_a}{d^3 \rho_a^0} \tag{30}$$

In the fluid solver and flexible-structure solver, the predictor-corrector scheme is used for time integration.

3 SIMULATION RESULTS

The filament movement in the coming flow is simulated. The length of the filament is L. A computational domain of extent [-2.5L,6.875L]×[-1.875L,1.875L] is employed in the present work. The filament is positioned within the computational domain, fixed at its left end, while the right end is free. Initially, the filament is placed in an orientation angle $\theta = 0.1\pi$ to the direction of the constant incoming flow and gravity $\boldsymbol{g}$, as shown in Figure 1. The dimensionless parameters are chosen as $Re = \frac{\rho^f U_0 L}{\mu} = 200$, $\lambda = \frac{\rho^s d}{\rho^f L} = 1.5$, $K_B = \frac{EI}{\rho^f {U_0}^2 L^3} = 0.0015$, $Fr = \frac{u}{\sqrt{gL}} = 1.4$. The initial turbulent kinetic energy is set to k=0.00489$U_0{}^2$, and the initial dissipation rate is set to $\mu_t = 57\mu$. The SPH particles are uniformly distributed with spacing $\Delta = 0.009375L$. The GPU parallel algorithm is used to enhance computational efficiency.

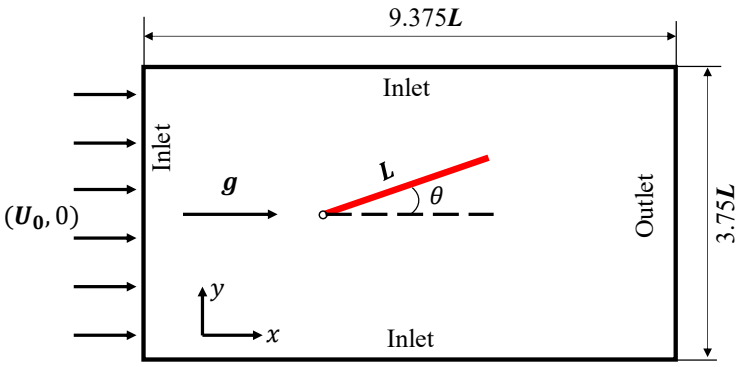

Figure 1: Computational model of the single flapping filament in uniform flow.

The results of filament motion and the flow field are obtained using the current SPH algorithm. Figure 2 shows the instantaneous velocity and vorticity contours at several moments. It can be seen that as time goes by, the vortex sheds from the filament and gradually decreases in intensity as it moves back. At the same time, the filament is flapping symmetrically and periodically. The obtained results illustrate the feasibility of the current SPH algorithm in simulating FFSI problems.

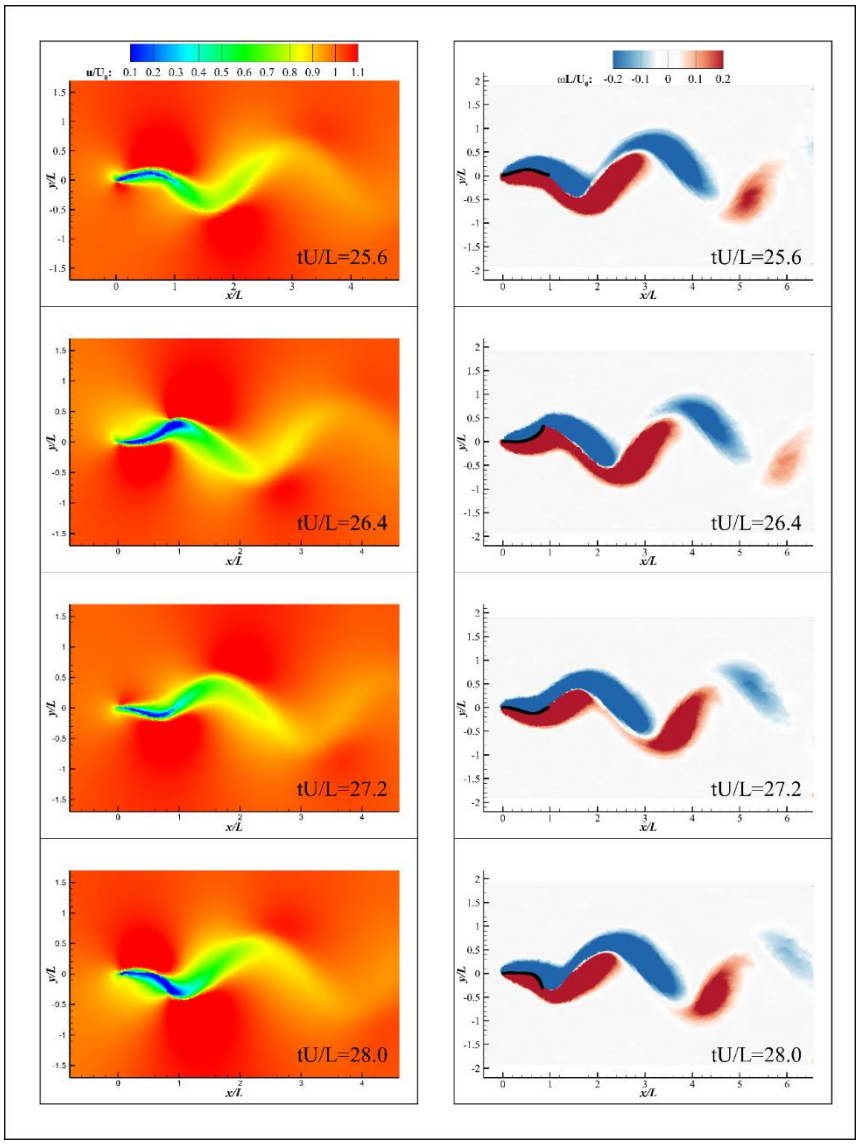

Figure 2: Dimensionless velocity contours and vorticity contours for fully developed flow at tU_0/L=25.6, 26.4, 27.2, and 28.0.

4 CONCLUSIONS

- To simulate the FFSI problems, a pure SPH method is proposed to discretize both the fluid dynamics equations and the structural dynamics equations. In the pure SPH method, the shell model is used to simulate the thin structure, and a single-layer boundary is combined into the shell model to avoid the error caused by the boundary truncation.
- The proposed SPH algorithm can simulate the FFSI problems stably. The motion of the filament and the flow field are captured.

REFERENCES

[1] Wu, D. Zhang, C. Hu, X. An SPH formulation for general plate and shell structures with finite deformation and large rotation, *J. Comput. Phys.* (2024) **510**: 113113.

[2] Li, S.-B. Zhang, A.-M. Xiao,J.-P. Peng, Y.-X. Li, M.-K. An algorithm for implementing a boundary viscous force with single-layer wall particles based on WCSPH, *J. Comput. Phys* (2022) **464:**111328.

[3] Wang,S. and Yin, X. A numerical method to simulate the coupled oscillations of flexible structures in flowing fluids, *Chin. Sci. Bull.* (2010) **55**: 3880–3888.

[4] Wu, D. Zhang, C. Tang, X. Hu, X. An essentially non-hourglass formulation for total Lagrangian smoothed particle hydrodynamics, *Comput. Methods Appl. Mech. Eng.* (2023) **407**: 115915.

[5] Hu, D. Long, T. Xiao, Y. Han, X. Gu, Y. Fluid–structure interaction analysis by coupled FE–SPH model based on a novel searching algorithm, *Comput. Methods Appl. Mech. Eng.* (2014) **276**: 266–286.

[6] Ming, F.R. Zhang, A.M. Xue, Y.Z. Wang, S.P. Damage characteristics of ship structures subjected to shockwaves of underwater contact explosions, *Ocean Eng.* (2016) **117**: 359–382.

[7] Long, T. Hu, D. Yang, G. Wan, D. A particle-element contact algorithm incorporated into the coupling methods of FEM-ISPH and FEM-WCSPH for FSI problems, *Ocean Eng.* (2016) **123**:154-163

[8] Serván-Camas, B. Cercós-Pita, J.L. Colom-Cobb, J. García-Espinosa, J. Souto-Iglesias, A. Time domain simulation of coupled sloshing–seakeeping problems by SPH–FEM coupling, *Ocean Eng.* (2016) **123**: 383–396.

[9] O'Connor, J. and Rogers, B.D. A fluid–structure interaction model for free-surface flows and flexible structures using smoothed particle hydrodynamics on a GPU, *J. Fluids Struct.* (2021) **104**: 103312.

[10] Antoci, C. Gallati, M. Sibilla, S. Numerical simulation of fluid–structure interaction by SPH, *Comput. Struct.* (2007) **85**: 879–890.

[11] Han, L. and Hu, X. SPH modeling of fluid-structure interaction, *J. Hydrodyn* (2018) **30**: 62–69.

[12] Khayyer, A. Shimizu, Y. Gotoh, H. Hattori, S. Multi-resolution ISPH-SPH for accurate and efficient simulation of hydroelastic fluid-structure interactions in ocean engineering, *Ocean Eng.* (2021) **226**: 108652.

[13] Zhang, C. Rezavand, M. Hu, X. A multi-resolution SPH method for fluid-structure interactions, *J. Comput. Phys.* (2021) **429**: 110028.

[14] Sun, P.-N. Le Touzé, D. Oger, G. Zhang, A.-M. An accurate FSI-SPH modeling of challenging fluid-structure interaction problems in two and three dimensions, *Ocean Eng.* (2021) **221**: 108552.

[15] Liu, M.B. and Liu, G.R. Smoothed Particle Hydrodynamics (SPH): an Overview and Recent Developments, *Arch. Computat. Methods Eng.* (2010) **17**: 25–76.

[16] Monaghan, J.J. Smoothed Particle Hydrodynamics, *Annu. Rev. Astron. Astr.* (1992) **30**: 543–574.

[17] Wang, S. Hu, J. Huang, C. Yu, Y. Graphics processing unit-accelerated smoothed particle hydrodynamics—Finite difference method and the application for the flow around a cylinder with forced motions, *Phys. Fluids* (2021) **33**: 127122.
[18] Zhu, L. and Peskin, C.S. Simulation of a Flapping Flexible Filament in a Flowing Soap Film by the Immersed Boundary Method, *J. Comput. Phys.* (2002) **179**: 452–468.
[19] Monaghan, J.J. Simulating Free Surface Flows with SPH, *J. Comput. Phys.* (1994) **110**: 399–406.
[20] Huang, C. Zhang, D.H. Shi, Y.X. Si,Y.L. Huang, B. Coupled finite particle method with a modified particle shifting technology, *Int. J. Numer. Methods Eng.* (2018) **113**: 179–207.
[21] Bao, T. Hu, J. Huang, C. Yu, Y. Smoothed particle hydrodynamics with κ - ε closure for simulating wall-bounded turbulent flows at medium and high Reynolds numbers, *Phys. Fluids* (2023) **35**: 085114.
[22] Antuono, M. Colagrossi, A. Marrone, S. Molteni, D. Free-surface flows solved by means of SPH schemes with numerical diffusive terms, *Comput. Phys. Commun.* (2010) **181**: 532–549.
[23] Xu, R. Stansby, P. Laurence, D. Accuracy and stability in incompressible SPH (ISPH) based on the projection method and a new approach, *J. Comput. Phys.* (2009) **228**: 6703–6725.